ChemComm

COMMUNICATION

View Article Online
View Journal | View Issue

Cite this: *Chem. Commun.*, 2016, 52, 9691

Received 16th March 2016,
Accepted 3rd July 2016

DOI: 10.1039/c6cc02291j

www.rsc.org/chemcomm

Revealing instability and irreversibility in nonaqueous sodium–O_2 battery chemistry†

Sayed Youssef Sayed,‡[a] Koffi P. C. Yao,[b] David G. Kwabi,[b] Thomas P. Batcho,[c] Chibueze V. Amanchukwu,[d] Shuting Feng,[d] Carl V. Thompson[c] and Yang Shao-Horn*[abc]

Charging kinetics and reversibility of Na–O_2 batteries can be influenced greatly by the particle size of NaO_2 formed upon discharge, and exposure time (reactivity) of NaO_2 to the electrolyte. Micrometer-sized NaO_2 cubes formed at high discharge rates were charged at smaller overpotentials compared to nanometer-sized counterparts formed at low rates.

Metal–air batteries have received immense research attention due to their potential for utilization of oxygen from ambient air and higher theoretical gravimetric energy densities than the state-of-the-art Li-ion batteries (*e.g.* ~3500 W h $kg_{Li_2O_2}^{-1}$ [1,2] for a two-electron oxygen reduction reaction to form Li_2O_2 in Li–O_2 batteries[2,3] *vs.* ~600 W h kg_{cell}^{-1} in lithium-ion systems[1,4,5]). Unfortunately, significant device-level challenges exist in Li–O_2 battery technologies[6,7] including high charging overpotential (~1000 mV) during the oxygen evolution reaction (OER) and thus low voltage efficiencies (62%),[7,8] which have been attributed largely to the reactivity of the discharge reaction between the intermediate LiO_2 and product Li_2O_2 with electrolytes.[9,10]

In contrast to the Li–O_2 reaction kinetics, the one-electron oxygen reduction reaction (ORR) to form NaO_2 (at 2.27 V *vs.* Na/Na^+)[11–13] can be highly reversible, enabling high voltage efficiency (>87%)[14,15] with low OER overpotentials (~200 mV)[12,13,15,16] for Na–O_2 batteries. McCloskey *et al.*[13] have related the low overpotential during charging to the low reactivity of NaO_2 toward an ether-based electrolyte (DME) compared to Li_2O_2, and the relatively smaller quantities of parasitic species such as Na_2CO_3 (in Na–O_2 battery), whereas Li_2CO_3 build-up (in Li–O_2 battery) formed as a result of the electrochemical activity of Li_2O_2 toward the electrolyte and carbon electrode accounts for the high overpotential during Li_2O_2 oxidation. In this study, we report that the reactivity of NaO_2 with an ether-based electrolyte (1,2 dimethoxyethane, DME) is highly dependent on the size of NaO_2 particles formed and the time of exposure to the electrolyte: the smaller the size of NaO_2 formed upon discharge, and the longer the exposure to the electrolyte, the less reversible and greater the overpotential of the oxygen electrode upon charging. The results show that the charging kinetics of Na–O_2 batteries can be reduced greatly by the reactivity between NaO_2 and the ether-based electrolyte.

In our study, we used carpets of highly porous carbon nanotubes (CNTs) made by chemical vapour deposition as the oxygen electrode for Na–O_2 cells.[9,17] At a galvanostatic rate of 10 or 1000 mA g_c^{-1}, NaO_2 was confirmed as the discharge product of Na–O_2 cells in 0.1 M $NaClO_4$/DME (Fig. S1 and S2, ESI†). The NaO_2 cubes formed at 10 mA g_c^{-1} (~200 nm, Fig. 1a and Fig. S3, ESI†) were considerably smaller by more than one order of magnitude and thus had a greater specific surface area than those formed at 1000 mA g_c^{-1} (~3 μm, Fig. 1b), which is consistent with a previous work.[17] Here we show that charging voltage profiles of electrodes discharged at 10 mA g_c^{-1} and 1000 mA g_c^{-1} are considerably different, as shown in Fig. 1c. Although the charging potentials after 10 mA g_c^{-1} discharge/charge were lower (2.31 V *vs.* Na/Na^+) than those at 1000 mA g_c^{-1} (2.75 V *vs.* Na/Na^+), the charging plateau only lasted for 60% of the discharge capacity before rising sharply. However, in the case of 1000 mA g_c^{-1} discharge, 90% of the discharge capacity was recovered at the charging plateau. To further support the hypothesis that the greater flat-plateau charge capacity during 1000 mA g_c^{-1} charging is associated with large NaO_2 particles formed upon discharge, we discharged Na–O_2 cells at 10 mA g_c^{-1} followed by charging at 1000 mA g_c^{-1} and *vice versa* (Fig. 1c and the inset). As the flat-plateau charge capacity in that case was similar to that of 10 mA g_c^{-1} charging after 10 mA g_c^{-1} discharge, we hypothesize that the NaO_2 particle size formed upon discharge rather than the charging rate determines the charging potential profile and the capacity obtainable at 2.75 V *vs.* Na/Na^+, as shown in Fig. 1c.

[a] *The Research Laboratory of Electronics and the Electrochemical Energy Laboratory, Massachusetts Institute of Technology, 77 Massachusetts Avenue, Cambridge, MA 02139, USA. E-mail: shaohorn@mit.edu*
[b] *Department of Mechanical Engineering, Massachusetts Institute of Technology, 77 Massachusetts Avenue, Cambridge, MA 02139, USA*
[c] *Department of Materials Science and Engineering, Massachusetts Institute of Technology, 77 Massachusetts Avenue, Cambridge, MA 02139, USA*
[d] *Department of Chemical Engineering, Massachusetts Institute of Technology, 77 Massachusetts Avenue, Cambridge, MA 02139, USA*

† Electronic Supplementary Information (ESI) available. See DOI: 10.1039/c6cc02291j

‡ Permanent address: Department of Chemistry, Faculty of Science, Cairo University, Giza 12613, Egypt.

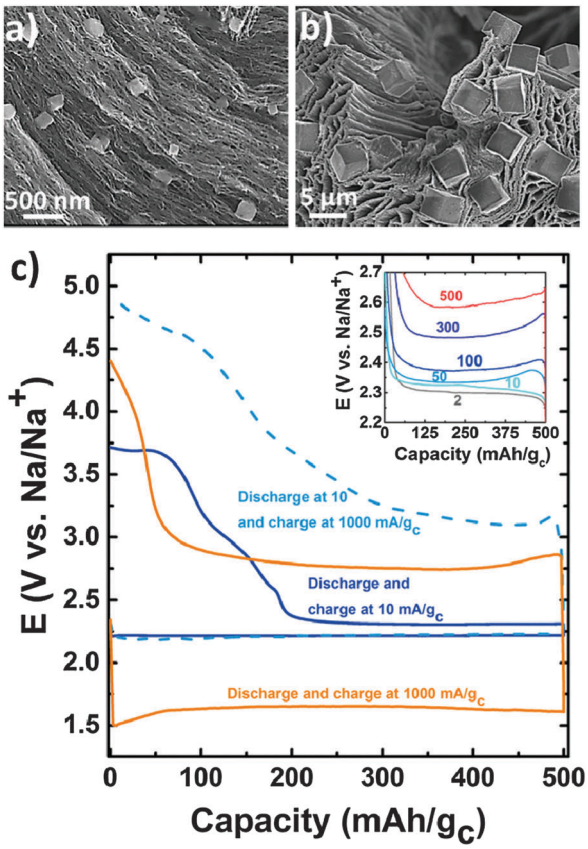

Fig. 1 (a) and (b) SEM images for discharged cathodes (CNTs) for Na–O_2 cells in 0.1 M $NaClO_4$/DME at 10 and 1000 mA g_c^{-1}, respectively. (c) Discharge–charge profiles for Na–O_2 cells at galvanostatic rates of 10 and 1000 mA g_c^{-1}. The solid lines are for using the same rate in discharge and charge. The dashed line is for a cell discharged at 10 mA g_c^{-1} and charged at 1000 mA g_c^{-1}. The inset in (c) shows voltage *vs.* capacity of CNT electrodes charged galvanostatically between 2 and 500 mA g_c^{-1} to 500 mA h g_c^{-1}; these electrodes were discharged galvanostatically at 1000 mA g_c^{-1}.

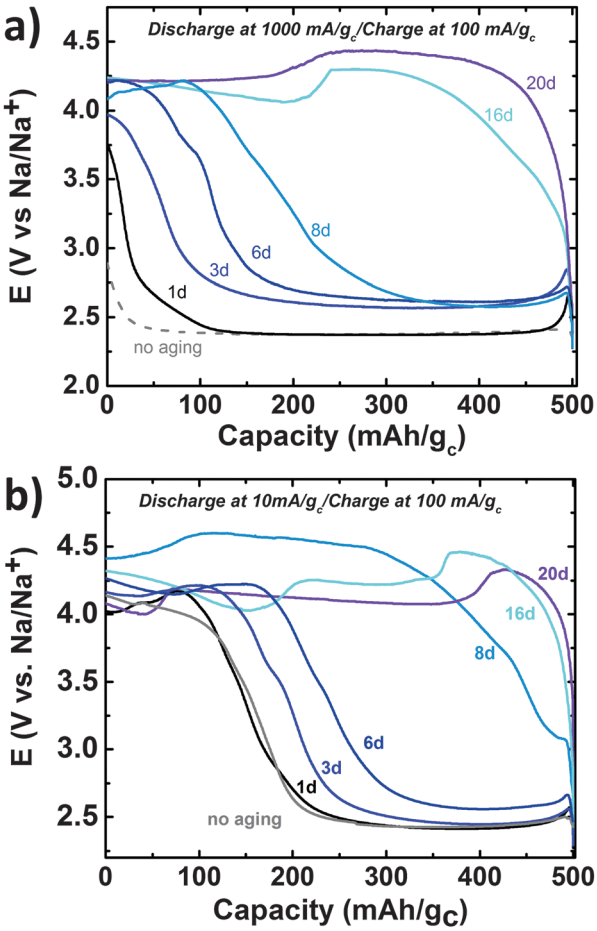

Fig. 2 Galvanostatic charging at 100 mA g_c^{-1} for Na–O_2 cells aged at different days after discharging in 0.1 M $NaClO_4$/DME at (a) 1000 and (b) 10 mA g_c^{-1} to 500 mA h g_c^{-1}.

This hypothesis is supported by the observation that one charging plateau was observed for electrodes discharged at 1000 mA g_c^{-1}, regardless of the charging rate (inset of Fig. 1c). We propose that the capacity obtainable on the lowest-voltage plateau (<3.00 V *vs.* Na/Na^+) upon charge originates from the reactivity of different NaO_2 particle sizes with the electrolyte. It is worth noting that the discharge time can also influence the reactivity of NaO_2 with the electrolyte, which is 50 h for nanometer-size particles formed at 10 mA g_c^{-1} compared to 0.5 h for the growth of micrometer particles. Having more contact time with the electrolyte for smaller particles upon discharge led to smaller charge capacities without aging, as shown in Fig. 2. Smaller NaO_2 particles formed at low discharge rates with a high specific surface area can react with the electrolyte to produce greater parasitic products per unit volume of NaO_2 or per discharge capacity, which requires high over-potentials to oxidize upon charging. On the other hand, larger NaO_2 particles, with less parasitic products per unit volume of NaO_2 or per discharge capacity were found to have greater capacity on the charging plateau characteristic of NaO_2 oxidation.[11] We propose that charging at the sloping voltage region results from the parasitic reaction products between NaO_2 and the electrolyte. Potential parasitic products may include $Na_2O_2{\cdot}2H_2O$, $NaOH_{(solid)}$, $NaOH_{(aqueous)}$, $Na_2CO_{3(solid)}$, $Na_2CO_{3(aqueous)}$, which have oxidation potentials of 2.33 V, 2.70 V, 3.11 V, 3.41 V, and 3.45 V *vs.* Na/Na^+,[18] respectively, all higher than that of NaO_2 (2.27 V).[15] The details will be discussed below.

The galvanostatic intermittent titration technique (GITT) was employed to determine the quasi-equilibrium potential during electrochemical oxidation[19] of NaO_2 cubes. The GITT charging of NaO_2 formed either at 1000 and 10 mA g_c^{-1} (Fig. S4a, ESI†) gave rise to an open-circuit voltage plateau at ~2.27 V *vs.* Na/Na^+, which is characteristic for NaO_2.[15] The capacities of the charging plateau for NaO_2 oxidation before the onset of potential rise were 325 mA h g_c^{-1} (16 days upon charge) and 120 mA h g_c^{-1} (6 days) for cells discharged at 1000 mA g_c^{-1} (30 min upon discharge) and 10 mA g_c^{-1} (50 h upon discharge), respectively (Fig. S4, ESI†). The efficient charging of larger NaO_2 cubes from the GITT is in agreement with Fig. 1c, which further supports the claim that the stability of NaO_2 in the electrolyte and the amount of parasitic reaction products are highly dependent on its particle size.

We further used the potentiostatic intermittent titration technique (PITT), which reveals the minimum overpotential required to drive two-phase oxidation,[20–22] to support findings of the GITT. A voltage plateau, spanning a capacity of 210 mA h g_c^{-1}, occurs at 2.25 V *vs.* Na/Na^+ for large NaO_2 particles formed at

1000 mA g_c^{-1} (Fig. S5, ESI†), which is close to the quasi-equilibrium potential (2.27 V *vs.* Na/Na^+), indicative of fast electrochemical oxidation kinetics of NaO_2. In Li–O_2 batteries, however, ~400 and 500 mV were determined by the PITT as the minimum overpotential for the oxidation of Li_2O_2 on CNT[21] and on Vulcan Carbon,[23] respectively. The fast OER kinetics for NaO_2 is substantiated by the high exchange current density of 7.6 nA cm^{-2} (Fig. S6, ESI†), which is ~2 orders of magnitude higher than 0.04 nA cm^{-2} obtained for electrochemical oxidation of Li_2O_2 discs[21] on CNTs. The capacity of the initial voltage plateau spanned 210 mA h g_c^{-1} after 16 days of charging, which is similar to the amount of time required for the equilibrium potential measured by GITT to diverge significantly from 2.27 V (Fig. S4a, ESI†). This highlights again the sensitivity of NaO_2 oxidation to electrolyte reactivity, *vide infra*. We propose that the plateau at 3.20 V *vs.* Na/Na^+ found in the PITT measurements corresponds to the oxidation of NaOH (thermodynamic potential of $NaOH_{Solid}$ is 3.11 V *vs.* Na/Na^+).[18] The decomposition of NaOH has been observed at 3.15 V *vs.* Na/Na^+ by Zhao *et al.* and was related to the decomposition of $Na_2O_2{\cdot}2H_2O \rightarrow 2NaOH + H_2O + 1/2O_2$.[18]

In order to examine the effect of NaO_2-electrolyte exposure time on the charging kinetics, we discharged Na–O_2 cells to 500 mA h g_c^{-1} at rates of 1000 and 10 mA g_c^{-1} (Fig. 2) and aged them in contact with the electrolyte at OCV from 1 to 20 days, followed by charging at a galvanostatic rate of 100 mA g_c^{-1}. For electrodes discharged at 1000 and 10 mA g_c^{-1}, aging up to 20 days led to a significant loss in the charging capacity for the low-voltage plateau (<3.00 V *vs.* Na/Na^+) characteristic of NaO_2 oxidation. A low capacity loss was noted for electrodes with larger NaO_2 particles discharged at 1000 mA g_c^{-1} relative to the smaller ones discharged at 10 mA g_c^{-1} for any given aging time (Fig. 2a and b). Of significance to note that larger NaO_2 particles can be charged with an efficiency of 46% for the low-voltage plateau (<3.00 V *vs.* Na/Na^+) after 8 days of aging compared to 0% for the cells discharged at 10 mA g_c^{-1}, Fig. S7 (ESI†). Electrochemical Impedance Spectroscopy (EIS) further revealed that the increased charging overpotentials with aging originated from increased charge transfer resistance at the oxygen electrode, especially from 0 to 4 days of aging (Fig. S8 and Table S1, ESI†). The charge transfer resistance increased tenfold from ~6.3 kΩ after discharge to ~62.3 kΩ for electrodes discharged at 1000 mA g_c^{-1} after 20 days of aging. Changes in the impedance from the pristine CNT cathode (Fig. S9, ESI†) and Na anode (Fig. S10, ESI†) alone were comparatively negligible.

We now discuss morphological and chemistry changes of NaO_2 discharged at 1000 mA g_c^{-1} during aging for 20 days, where the discharged electrode was left in contact with the electrolyte at OCV. Fig. 3a shows the effect of aging for 20 days on the charging kinetics at 2 mA g_c^{-1} for an electrode discharged at 1000 mA g_c^{-1}. While the unaged cell showed a flat voltage plateau at ~2.30 V *vs.* Na/Na^+ spanning >90% of the capacity, the aged cell showed a monotonous increase in the voltage at the initial stage of charging, followed by sloping regions up to 50% of the capacity and finally a voltage plateau at 3.37 V, in agreement with the PITT measurements after 16 days of charging (Fig. S5, ESI†). The effect of aging on the morphology of the NaO_2 cubes was noted clearly in the SEM image shown in the top inset in Fig. 3a, where the NaO_2 surfaces

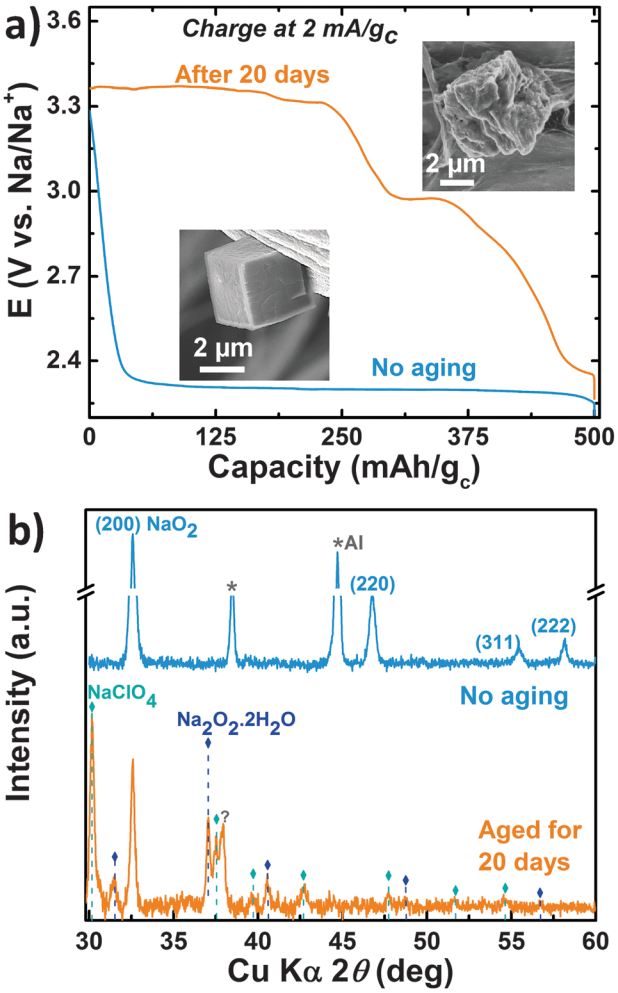

Fig. 3 (a) Charging profiles at 2 mA g_c^{-1}, without and after aging for 20 days, for Na–O_2 cells discharged to 500 mA h g_c^{-1} at 1000 mA g_c^{-1} in 0.1 M $NaClO_4$/DME. The inset shows the SEM images for NaO_2 cubes before (bottom) and after (top) aging. (b) XRD for Na–O_2 electrodes before and after aging for 20 days.

are roughened compared to smoother cubic particles before aging (bottom inset in Fig. 3a). The XRD measurements (Fig. 3b) on the aged electrode showed $Na_2O_2{\cdot}2H_2O$ *versus* the NaO_2 seen in the discharged electrode without aging. A Raman signal at 1156 cm^{-1} was observed for the unaged electrode (Fig. S11, ESI†), indicating the formation of NaO_2. However, the aged electrode showed a Raman peak at 1147 cm^{-1}. In anhydrous Na_2O_2, two sharp peaks at 738 and 794 cm^{-1} were observed in addition to a peak at 1141 cm^{-1}, which was assigned to remnant quantities of superoxide.[24] However, the peak at 1147 cm^{-1} is also close to the computed torsion and stretching modes from CH_3O and C–O groups, consistent with the presence of sodium methoxide or sodium methyl carbonate-type decomposition products.[25]

Here we point out that the reactivity of NaO_2 with the electrolyte (DME) observed in this study is markedly different from that reported recently by Kim *et al.*[26] This previous study reveals $Na_2O_2{\cdot}2H_2O$ from Raman spectroscopy immediately after discharge in diethylene glycol dimethyl ether (diglyme) containing $NaCF_3SO_3$ in contrast to only NaO_2 found in this

work. Moreover, aging for 12 hours greatly reduces the capacity (~85% lost) for the low-voltage plateau (<3.00 V *vs.* Na/Na^+) characteristic for NaO_2 oxidation during charging of ~30 μm-sized NaO_2 particles in the previous work, while our work shows that aging for more than 10 days is needed to result in a comparable loss for ~3 μm-sized NaO_2 particles. The origin of this discrepancy is unknown, and it could be due to the use of different electrolytes (solvent and/or salt), degrees of cell sealing against ambient atmosphere, or native impurities in the electrolytes.[27]

We propose a mechanism for NaO_2 degradation and $Na_2O_2 \cdot 2H_2O$ formation in Fig. S12 (ESI†). The first step of the reaction (1) is hydrogen abstraction from DME in the presence of O_2^-,[28] similar to what has been recently proposed for the oxidation of poly(ethylene) oxide,[29] and DME degradation in Li–O_2 electrochemistry.[28] We note that this step has been considered likely from recent computational studies of DME stability,[30] in contrast to proton abstraction, which Kim *et al.*[26] proposed for DME degradation. Reaction (1) produces HO_2^- and a DME radical ($CH_3C^{\bullet}HCH_2OCH_3$), which can initiate a chain reaction when the radical reacts with O_2 (2) to produce more DME radicals (3) and OH^- ions (4). Meanwhile HO_2^- can disproportionate in the presence of Na^+ ions in the electrolyte to produce Na_2O_2 and H_2O_2 (6). The latter can combine with OH^- ions produced in (4) and Na^+ ions to form $Na_2O_2 \cdot 2H_2O$ *via* the peroxo-hydroxylation (10) reaction proposed by Kim *et al.*[26]

To summarize, we have studied the effect of the discharge rate on the particle size of NaO_2, which has shown to play a key role in the kinetics of the subsequent OER. After discharge at 1000 mA g_c^{-1}, ~3 μm-sized NaO_2 particles are observed compared to ~200 nm after discharge at 10 mA g_c^{-1}. Subsequent charging studies show that the larger ~3 μm NaO_2 particles can be oxidized at <3.00 V *vs.* Na/Na^+ for higher capacities than the smaller ~200 nm NaO_2. These results highlight the effect of the particle size on the OER kinetics. PITT experiments revealed intrinsically fast kinetics for the oxidation of NaO_2, while aging NaO_2 in contact with the electrolyte has explicitly shown that NaO_2 can react with the electrolyte significantly over time, resulting in markedly reduced charging kinetics and irreversibility.

S. Y. S. D. G. K. and T. B. were supported in part by the Skoltech-MIT Center for Electrochemical Energy Storage. S. Y. S. acknowledges the support of a postdoctoral fellowship from the Natural Sciences and Engineering Research Council (NSERC) of Canada. D. G. K. was also supported by the China Clean Energy Research Center-Clean Vehicles Consortium, and the US Department of Energy (under award number DE-PI00000012). K. P. C. Y. was supported by Toyota Motor Europe. C. V. A. was supported by the US Department of Defense through the National Defense Science and Engineering Graduate (NDSEG) Fellowship and the GEM Fellowship. Shuting Feng was supported by the Samsung Advanced Institute of Technology (SAIT). The authors would like to thank Dr Nagore Ortiz-Vitoriano for her help in capturing the SEM images (Fig. 1a and Fig. S3, ESI†) and valuable discussions. Imaging was performed at the Center for Nanoscale Systems (CNS) at the Harvard University.

Notes and references

1 D. G. Kwabi, N. Ortiz-Vitoriano, S. A. Freunberger, Y. Chen, N. Imanishi, P. G. Bruce and Y. Shao-Horn, *MRS Bull.*, 2014, **39**, 443–452.
2 P. G. Bruce, S. A. Freunberger, L. J. Hardwick and J. M. Tarascon, *Nat. Mater.*, 2012, **11**, 19–29.
3 L. Johnson, C. Li, Z. Liu, Y. Chen, S. A. Freunberger, P. C. Ashok, B. B. Praveen, K. Dholakia, J.-M. Tarascon and P. G. Bruce, *Nat. Chem.*, 2014, **6**, 1091–1099.
4 S. H. Oh and L. F. Nazar, *Adv. Energy Mater.*, 2012, **2**, 903–910.
5 H. Chen, M. Armand, G. Demailly, F. Dolhem, P. Poizot and J.-M. Tarascon, *ChemSusChem*, 2008, **1**, 348–355.
6 A. C. Luntz and B. D. McCloskey, *Chem. Rev.*, 2014, **114**, 11721–11750.
7 R. R. Mitchell, B. M. Gallant, C. V. Thompson and Y. Shao-Horn, *Energy Environ. Sci.*, 2011, **4**, 2952–2958.
8 Y.-C. Lu, B. M. Gallant, D. G. Kwabi, J. R. Harding, R. R. Mitchell, M. S. Whittingham and Y. Shao-Horn, *Energy Environ. Sci.*, 2013, **6**, 750–768.
9 B. M. Gallant, R. R. Mitchell, D. G. Kwabi, J. Zhou, L. Zuin, C. V. Thompson and Y. Shao-Horn, *J. Phys. Chem. C*, 2012, **116**, 20800–20805.
10 B. D. McCloskey, A. Speidel, R. Scheffler, D. C. Miller, V. Viswanathan, J. S. Hummelshøj, J. K. Nørskov and A. C. Luntz, *J. Phys. Chem. Lett.*, 2012, **3**, 997–1001.
11 P. Hartmann, M. Heinemann, C. L. Bender, K. Graf, R.-P. Baumann, P. Adelhelm, C. Heiliger and J. Janek, *J. Phys. Chem. C*, 2015, **119**, 22778–22786.
12 C. Xia, R. Black, R. Fernandes, B. Adams and L. F. Nazar, *Nat. Chem.*, 2015, **7**, 496–501.
13 B. D. McCloskey, J. M. Garcia and A. C. Luntz, *J. Phys. Chem. Lett.*, 2014, **5**, 1230–1235.
14 P. Hartmann, C. L. Bender, J. Sann, A. K. Durr, M. Jansen, J. Janek and P. Adelhelm, *Phys. Chem. Chem. Phys.*, 2013, **15**, 11661–11672.
15 P. Hartmann, C. L. Bender, M. Vračar, A. K. Dürr, A. Garsuch, J. Janek and P. Adelhelm, *Nat. Mater.*, 2013, **12**, 228–232.
16 P. Adelhelm, P. Hartmann, C. L. Bender, M. Busche, C. Eufinger and J. Janek, *Beilstein J. Nanotechnol.*, 2015, **6**, 1016–1055.
17 N. Ortiz-Vitoriano, T. P. Batcho, D. G. Kwabi, B. Han, N. Pour, K. P. C. Yao, C. V. Thompson and Y. Shao-Horn, *J. Phys. Chem. Lett.*, 2015, **6**, 2636–2643.
18 N. Zhao, C. Li and X. Guo, *Phys. Chem. Chem. Phys.*, 2014, **16**, 15646–15652.
19 Z. H. Cui, X. X. Guo and H. Li, *Energy Environ. Sci.*, 2015, **8**, 182–187.
20 N. Meethong, H. Y. S. Huang, S. A. Speakman, W. C. Carter and Y. M. Chiang, *Adv. Funct. Mater.*, 2007, **17**, 1115–1123.
21 B. M. Gallant, D. G. Kwabi, R. R. Mitchell, J. Zhou, C. V. Thompson and Y. Shao-Horn, *Energy Environ. Sci.*, 2013, **6**, 2518–2528.
22 X. Ma, H. Chen and G. Ceder, *J. Electrochem. Soc.*, 2011, **158**, A1307–A1312.
23 Y.-C. Lu and Y. Shao-Horn, *J. Phys. Chem. Lett.*, 2013, **4**, 93–99.
24 J. C. Evans, *J. Chem. Soc. D*, 1969, 682–683, DOI: 10.1039/c29690000682.
25 R. S. Sanchez-Carrera and B. Kozinsky, *Phys. Chem. Chem. Phys.*, 2014, **16**, 24549–24558.
26 J. Kim, H. Park, B. Lee, W. M. Seong, H.-D. Lim, Y. Bae, H. Kim, W. K. Kim, K. H. Ryu and K. Kang, *Nat. Commun.*, 2016, **7**, DOI: 10.1038/ncomms10670.
27 K. U. Schwenke, S. Meini, X. Wu, H. A. Gasteiger and M. Piana, *Phys. Chem. Chem. Phys.*, 2013, **15**, 11830–11839.
28 B. D. Adams, R. Black, Z. Williams, R. Fernandes, M. Cuisinier, E. J. Berg, P. Novak, G. K. Murphy and L. F. Nazar, *Adv. Energy Mater.*, 2015, **5**, 1400867.
29 J. R. Harding, C. V. Amanchukwu, P. T. Hammond and Y. Shao-Horn, *J. Phys. Chem. C*, 2015, **119**, 6947–6955.
30 N. Kumar, M. D. Radin, B. C. Wood, T. Ogitsu and D. J. Siegel, *J. Phys. Chem. C*, 2015, **119**, 9050–9060.

